Static and dynamic stiffness analyses of cable-driven parallel robots with non-negligible cable mass and elasticity

Han Yuan, Eric Courteille, Dominique Deblaise

Static and dynamic stiffness analyses of cable-driven parallel robots with non-negligible cable mass and elasticity

Han Yuan, Eric Courteille *, Dominique Deblaise

Université Européenne de Bretagne, INSA-LGCGM-EA 3913, 20, avenue des Buttes de Cöesmes, 35043 Rennes Cedex, France

This paper focuses on the stiffness analysis of cable-driven parallel robots (CDPRs), including the static stiffness and the dynamic stiffness analyses. Static and dynamic cable models are introduced considering the effect of both cable mass and elasticity. Based on these models, the static stiffness of CDPRs is evaluated by the variation of the end-effector pose error, and the dynamic stiffness of CDPRs is analyzed by identifying the robot natural frequencies. Simulations and experiments are made on a 6-DOF prototype to validate the theoretical models. Comparison with other methods available in literature is presented. Results show the important effect of cable mass and elasticity on the static and dynamic stiffness of CDPRs.

1. Introduction

Cable-driven parallel robots (CDPRs) are a special variant of traditional rigid-link parallel robots. There are some advantages to use flexible cables instead of rigid links, such as high dynamics due to small moving mass, large workspace, and low cost [1]. However, as cables present the particularity of not being rigid and are only able to act in tension, the stiffness of CDPRs becomes a vital concern [2,3]. Stiffness performances have a significant effect on the static and dynamic behaviors of CDPRs, such as kinematics, positioning accuracy, force distribution, vibration and control [1,4]. Deficient static stiffness can decrease the positioning accuracy of CDPRs, and bad dynamic stiffness characteristics can lead to vibration and long settling time. Although stiffness has been well studied in the last few decades for rigid-link parallel robots [1,4–8], there is little literature on the stiffness problem of CDPRs.

When it comes to the static stiffness analysis of CDPRs, an important issue is cable modeling. Many studies used linear or non-linear spring as cable model [9–17]. This approach only considers the elasticity along cable axis and assumes cable as massless spring. This assumption is not accurate, especially for CDPRs with heavy and/or long-span cables. In fact, the axial cable stiffness is not the only source of the static stiffness. Sag-introduced stiffness should also be considered. Another well known model is the static sagging cable model derived from civil engineering [18]. It is used in several previous researches [2,3,19–21]. The sagging cable model considers the effect of cable mass and elasticity. It is more accurate than the spring cable model in the static stiffness analysis of CDPRs. In previous researches, the effect of cable sag on the static stiffness of CDPRs is verified [3,19,21]. However, to our best knowledge, the verification is limited to numerical investigations. Experimental verification of the static stiffness is only performed on a single sagging cable [18,19] but not on CDPRs.

Another issue for the static analysis is the index of stiffness performance evaluation. Most studies [9,10,21] use Cartesian stiffness matrix or its mathematical properties (such as determinant, trace, norm, and etc) as evaluation indices. For massless cable

* Corresponding author.
E-mail addresses: yuan.han.robot@gmail.com (H. Yuan), eric.courteille@insa-rennes.fr (E. Courteille), dominique.deblaise@insa-rennes.fr (D. Deblaise).

assumption, the static stiffness of CDPRs only depends on the axial stiffness of cables. In linear-elastic range, the axial stiffness is independent of cable forces. Thus the Cartesian stiffness matrix is independent of the external wrench applied to the end-effector. It is easy to compute the Cartesian stiffness matrix through the Jacobian matrix of CDPRs. However, with non-negligible cable mass, the cable profile between two attachment points is not a straight line but a sagging curve. So the direction of cable force is not along the chord of the curve but along the tangent line of the curve. In this case, Jacobian matrix cannot be used to calculate the Cartesian stiffness matrix, and partial differential equations should be employed instead. This increases calculation complexity. Furthermore, taking the cable sag into consideration, the stiffness of cables is relevant to cable forces and thus depends on the external wrench. Previous researches do not present the variation of the static stiffness with the external wrench.

Some applications of CDPRs require high performances, especially the dynamic performances. For examples: the ultrahigh speed FALCON robot [11,12], the wind-induced vibration problem of the large radio telescope [22] and the wind tunnels [23]. Vibration can be induced by initial position and velocity of the end-effector, wind disturbance, and/or friction of the cables around fixed pulleys [24]. Vibration can affect the positioning accuracy of the end-effector, and bring fluctuation on the trajectory. These applications lead to researches on the dynamic stiffness of CDPRs in recent years. Natural frequency is widely used in literature as an index for the dynamic stiffness evaluation of CDPRs [19,24–28]. Most of these researches [25,26,28] only consider cable elasticity, while neglect cable mass. Although cable mass is considered for the static analysis in [19], it is ignored in the computation of robot natural frequencies. As a matter of fact, in many situations, both cable mass and elasticity will affect system dynamics by changing the value of natural frequencies and/or adding new resonances. Therefore, both cable mass and elasticity should be taken into consideration for the dynamic analysis of CDPRs. The finite element cable model in [24,27] considers the effect of cable mass. This method uses distributed mass points and ideal lines between them to simulate continuous cable, but it leads to a system with partial differential equations. In addition, the accuracy of finite element method depends on the number of elements. To ensure a good accuracy will result in further computational complexity.

This paper focuses on the static and dynamic stiffness analyses of CDPRs. Static sagging cable model is introduced. This cable model considers cable mass and elasticity, and describes the static cable profile with a set of non-linear equations. Cable stiffness contains both axial flexibility and sag-introduced flexibility. Based on this sagging cable model, the variation of pose error with external load is used as an index for evaluating the static stiffness performance of CDPRs. The pose error of the end-effector can be calculated through the kinematic model of CDPRs. Based on this method, the static stiffness of CDPRs is analyzed by both simulations and experiments on a 6-DOF CDPR prototype. The effect of cable sag on the static stiffness is validated by experiment for the first time. The variation of the static stiffness with external load is presented.

A new dynamic stiffness model of CDPRs is proposed in this paper. This model is based on the Dynamic Stiffness Matrix (DSM) method. DSM is used to solve the vibration problems of structures. It is often regarded as an exact method, because DSM is based on the exact shape functions obtained from the exact solution of the element differential equations [29]. This method provides better accuracy compared with finite element method. Firstly, the dynamic stiffness matrix of a single cable proposed by [30,31] is introduced in this paper. This dynamic cable model considers the effect of cable mass and elasticity. Then the dynamic stiffness matrix of CDPRs is deduced, considering the coupling between end-effector vibration and cable vibration. The dynamic response functions of CDPRs are achieved to identify the system natural frequencies. In addition, experiments on a 6-DOF CDPR prototype are performed to verify the proposed dynamic stiffness model. The Frequency Response Functions of the prototype are calculated, and natural frequencies are identified. Experimental results are also compared with other methods available in literature.

This paper is organized as follow. Static cable model and dynamic cable model are firstly introduced in Section 2. Then the static and dynamic stiffness analyses of CDPRs are presented in Section 3. In this section, the kinematic model of CDPRs is set up. Based on this model, the pose error of CDPRs is defined, and the variation of the end-effector pose error with the external load is regarded as an index for the static stiffness evaluation. The dynamic stiffness matrix of CDPRs is formulated, and dynamic response functions are deduced to identify the natural frequencies. Section 4 presents a 6-DOF CDPR prototype. Simulations and experiments are carried out to investigate the static and dynamic stiffness performance of the prototype. Section 5 analyzes the stiffness characteristics of the prototype over its workspace. Applications of the proposed method on the design procedures of suspended CDPRs and non-suspended CDPRs are discussed. Finally, conclusions are made in Section 6.

2. Cable modeling

Cable modeling is the basis of the stiffness analysis of CDPRs. In this section, the static sagging cable model and the DSM cable model are introduced. Compared with massless spring model, the proposed cable models considering both cable mass and elasticity are more accurate in describing the static and dynamic cable behavior.

2.1. Static cable model

The static sagging cable model, also known as elastic catenary model, considers the effect of both cable mass and elasticity. It gives the static cable profile by a set of non-linear equations. This model has been studied and used in civil engineering since 1930s [18]. However, it is quite new in the analysis of CDPRs [3]. In addition, this cable model is the theoretical basis of this paper. It is necessary to briefly introduce this model with variables familiar to robotics.

The diagram of an inclined cable is presented in Fig. 1. One of the cable-ends is fixed, and an external force is applied to the other end. With the effect of both external force and gravity, the shape of the cable between points **A** and **B** is not a straight line, but a sagging curve in the *xOz* plane.

Assuming that **P** is an arbitrary point on the cable, the constraints for a differential cable element around the point **P** are:

1. The geometric constraint:

$$\left(\frac{dx}{dp}\right)^2 + \left(\frac{dz}{dp}\right)^2 = 1. \tag{1}$$

2. The constraint of static equilibrium:

$$f_P \frac{dx}{dp} = f_{Px} = f_{Ax}, \tag{2}$$

$$f_P \frac{dz}{dp} = f_{Pz} = f_{Az} - \rho g(l_{us} - s). \tag{3}$$

3. The constraint according to Hooke's law:

$$f_P = EA\left(\frac{dp}{ds} - 1\right). \tag{4}$$

where:

- (x, z) is the Cartesian coordinate of point **P** in frame $\mathfrak{R}_O(O, x, y, z)$;
- l_{us} and l_s are the unstrained and strained cable length between points **A** and **B** respectively;
- s and p are the Lagrangian coordinate in the unstrained and strained cable profile respectively, where $0 \le s \le l_{us}$ and $0 \le p \le l_s$;
- f_A is the cable force on point **A**; f_{Ax} and f_{Az} are the components of f_A along x and z axis respectively;
- f_P is the cable force on point **P**; f_{Px} and f_{Pz} are the components of f_P along x and z axis respectively;
- ρ is the cable mass per unit length;
- g is the gravitational acceleration;
- A is unstrained cross section area;
- E is the Young's modulus.

According to Eqs. (1) to (3), the force on point **P** can be written as:

$$f_P = \sqrt{f_{Px}^2 + f_{Pz}^2} = \sqrt{f_{Ax}^2 + [f_{Az} - \rho g(l_{us} - s)]^2}. \tag{5}$$

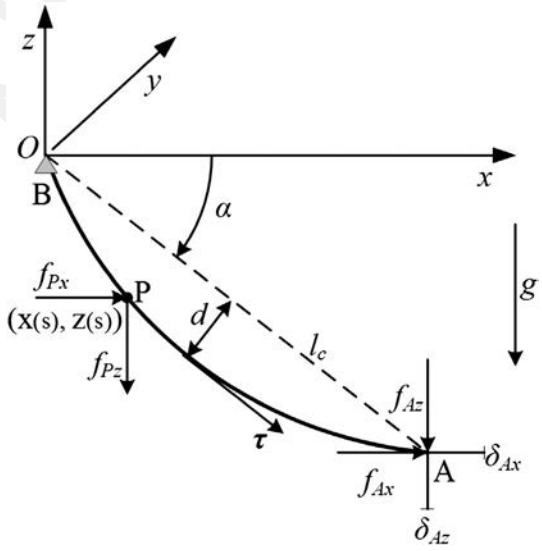

Fig. 1. Diagram of a sagging cable.

As $\frac{dx}{ds} = \frac{dx}{dp}\frac{dp}{ds}$, both $\frac{dx}{dp}$ and $\frac{dp}{ds}$ can be written as functions of f_P by Eqs. (2) and (4), $\frac{dx}{ds}$ can be written as:

$$\frac{dx}{ds} = \frac{dx}{dp}\frac{dp}{ds} = \frac{f_{Ax}}{f_P}\left(\frac{f_P}{EA} + 1\right). \tag{6}$$

Substituting Eq. (5) into Eq. (6) yields:

$$\frac{dx}{ds} = \frac{f_{Ax}}{EA} + \frac{f_{Ax}}{\sqrt{f_{Ax}^2 + [f_{Az} - \rho g(l_{us} - s)]^2}}. \tag{7}$$

Applying the same procedures for z-axis, we can get:

$$\frac{dz}{ds} = \frac{dz}{dp}\frac{dp}{ds} = \frac{f_{Pz}}{f_P}\left(\frac{f_P}{EA} + 1\right) = \frac{f_{Az} - \rho g(l_{us} - s)}{EA} + \frac{f_{Az} - \rho g(l_{us} - s)}{\sqrt{f_{Ax}^2 + [f_{Az} - \rho g(l_{us} - s)]^2}}. \tag{8}$$

After integration with the boundary condition $x(0) = 0$ and $z(0) = 0$, the static cable profile can be described as:

$$x(s) = \frac{f_{Ax}s}{EA} + \frac{|f_{Ax}|}{\rho g}\left\{sinh^{-1}\left[\frac{f_{Az} - \rho g(l_{us} - s)}{f_{Ax}}\right] - sinh^{-1}\left(\frac{f_{Az} - \rho g l_{us}}{f_{Ax}}\right)\right\}, \tag{9}$$

$$z(s) = \frac{f_{Az}s}{EA} + \frac{\rho g}{EA}\left(\frac{s^2}{2} - l_{us}s\right) + \frac{1}{\rho g}\left\{\sqrt{f_{Ax}^2 + [f_{Az} - \rho g(l_{us} - s)]^2} - \sqrt{f_{Ax}^2 + (f_{Az} - \rho g l_{us})^2}\right\}. \tag{10}$$

The sagging cable model considers both sag-introduced stiffness and axial stiffness. It describes the static cable profile with a set of non-linear equations.

2.2. Dynamic cable model

In this section, the dynamic model of a single cable is expressed in terms of the dynamic stiffness matrix. The Dynamic Stiffness Matrix method is an exact method providing good accuracy in the analysis of vibration problem. The dynamic stiffness matrix of an inclined cable is formulated in [29–31] by considering the cable mass, elasticity and damping. As presented in Fig. 1, the cable is considered as a continuum and its shape is given by l_c (the chord length), d (the sag perpendicular to the chord), and α (the inclination angle). According to [29–31], the following assumptions are made:

- The cable is assumed to be uniform;
- Only small displacements are admitted to meet the requirement of linear theory;
- Only small cable sag is allowed, where $\frac{d}{l_c}$ (the sag to span ratio) is no more than 1/20;
- Viscous damping is taken into consideration.

2.2.1. Dynamic stiffness matrix in 2 dimensions

For the sake of convenience, the dynamic stiffness matrix is firstly deduced in xOz plane (Fig. 1). The planar stiffness matrix $\mathbf{K}$ of a single sagging cable can be defined as the relationship between the forces $[f_{Ax}, f_{Az}]$ applied at the end point of the cable and the displacements $[\delta_{Ax}, \delta_{Az}]$ at the same point by Eq. (11). The displacements $[\delta_{Ax}, \delta_{Az}]$ are defined as differentials that represent small changes in position from static equilibrium.

$$\begin{bmatrix} f_{Ax} \\ f_{Az} \end{bmatrix} = \mathbf{K}\begin{bmatrix} \delta_{Ax} \\ \delta_{Az} \end{bmatrix} \tag{11}$$

According to [31], the stiffness matrix $\mathbf{K}$ of a planar sagging cable is a function of τ (the static cable tension at the section where the cable is parallel to the chord), c (the damping force per unit length and velocity), and ω (the frequency of harmonic motion). The expression of $\mathbf{K}$ is given by:

$$\mathbf{K}(\omega) = \begin{bmatrix} K_{xx}(\omega) & K_{xz}(\omega) \\ K_{zx}(\omega) & K_{zz}(\omega) \end{bmatrix}, \tag{12}$$

where:

$$K_{xx}(\omega) = k_a cos^2\alpha - 2k_b sin\alpha cos\alpha + k_c sin^2\alpha, \tag{13}$$

$$K_{xz}(\omega) = k_a cos\alpha sin\alpha - k_b sin^2\alpha + k_b cos^2\alpha - k_c sin\alpha cos\alpha, \tag{14}$$

$$K_{zx}(\boldsymbol{\omega}) = K_{xz}, \tag{15}$$

$$K_{zz}(\boldsymbol{\omega}) = k_a \sin^2\alpha + 2k_b \sin\alpha\cos\alpha + k_c \cos^2\alpha. \tag{16}$$

The relative parameters in the stiffness matrix **K** components are:

$$k_a(\boldsymbol{\omega}) = \frac{EA}{L_e}\frac{1}{1+\frac{\lambda^2}{\Omega_c^2}(\kappa-1)}, \tag{17}$$

$$k_b(\boldsymbol{\omega}) = \frac{EA}{L_e}\frac{\frac{1}{2}\varepsilon(\kappa-1)}{1+\frac{\lambda^2}{\Omega_c^2}(\kappa-1)}, \tag{18}$$

$$k_c(\boldsymbol{\omega}) = \frac{EA}{L_e}\frac{\varepsilon^2}{\lambda^2}\frac{1}{\kappa} - \frac{EA\frac{1}{4}\frac{\varepsilon^2}{\lambda^2}\Omega_c^2\left[\kappa+\frac{\lambda^2}{\Omega_c^2}(\kappa-1)\right]}{L_e \quad 1+\frac{\lambda^2}{\Omega_c^2}(\kappa-1)}, \tag{19}$$

where:

- $\lambda^2 = \left(\frac{\rho \mathbf{g} l_c}{\tau}\right)^2 \frac{EAl_c}{\tau L_e}\cos^2\alpha$ is the fundamental cable parameter which represents the elastic stiffness relative to the catenary stiffness, where l_c is the chord length and α is the inclination angle;
- $\varepsilon = \frac{\rho \mathbf{g} l_c}{\tau}\cos\alpha = \frac{8d}{l_c}$ is the ratio between horizontal cable weight and cable tension, where d is the sag perpendicular to the chord;
- $L_e = \int_0^{l_c}\left(\frac{ds}{dx}\right)^3 dx \simeq l_c\left[1+8\left(\frac{d}{l_c}\right)^2\right]$ is the cable length parameter;
- $\xi = \frac{c}{2\rho\omega}$ is the damping ratio;
- $\omega_c = \omega\sqrt{1-2\xi i}$ is the frequency–damping parameter;
- $\Omega = \omega l_c\sqrt{\frac{\rho}{\tau}}$ is the dimensionless frequency parameter;
- $\Omega = \omega_c l_c\sqrt{\frac{\rho}{\tau}}$ is the dimensionless frequency–damping parameter;
- $\kappa = \frac{\tan\left(\frac{\alpha}{2}\right)}{\left(\frac{\alpha}{2}\right)}$ is an auxiliary term.

2.2.2. Dynamic stiffness matrix in 3 dimensions

Similar to the deduction of the planar dynamic stiffness matrix, with the consideration of the out-of-plane motion (cable motion along *y*-axis), the spatial dynamic stiffness matrix in 3 dimensions can be expressed as:

$$\mathbf{K}^{3D}(\boldsymbol{\omega}) = \begin{bmatrix} K_{xx}(\boldsymbol{\omega}) & 0 & K_{xz}(\boldsymbol{\omega}) \\ 0 & K_{yy}(\boldsymbol{\omega}) & 0 \\ K_{zx}(\boldsymbol{\omega}) & 0 & K_{zz}(\boldsymbol{\omega}) \end{bmatrix}. \tag{20}$$

In linear theory the in-plane motion is uncoupled with the out-of-plane motion [29,30]. So the interaction coefficients in Eq. (20) are zeros. According to [29], the stiffness matrix coefficient for the out-of-plane motion is: $K_{yy}(\boldsymbol{\omega}) = \frac{\tau(4-\kappa^2\Omega_c^2)}{4\kappa l_c}$. The other coefficients are the same with those in Eq. (12).

2.2.3. Dynamics of an example cable

The coefficient of the dynamic stiffness matrix $K_{xx}(\boldsymbol{\omega})$ is calculated for an example cable whose properties are: $E = 20$ Gpa, $A = 1.26\times10^{-5}$ m^2, $l_c = 6.848$ m, $\tau = 77.6$ N, $\alpha = 36°$, $\xi = 0.003$. The relevant parameters are: $\frac{L_e}{l_c} = 1.0003 \approx 1$, $\lambda^2 = 7.57$ and $\varepsilon = 0.048$. For comparison, the coefficient of the equivalent static stiffness matrix for the same cable is calculated using the method presented in [19].

The amplitude variation of a coefficient (such as $K_{xx}(\boldsymbol{\omega})$) of the dynamic and static stiffness matrix is plotted with respect to the frequency of harmonic motion $\boldsymbol{\omega}$ in Fig. 2. As expected, the static stiffness coefficient is constant. However, the dynamic stiffness coefficient is variable with frequency. Considerable variations of the dynamic stiffness amplitude are present within the range of the natural frequencies, and these variations are associated with symmetric and antisymmetric modes of the cable. Therefore, the contribution of the cable dynamics and the coupling between the cable vibration and the end-effector vibration should be considered in the dynamic stiffness analysis of CDPRs.

3. Stiffness analysis of CDPRs

3.1. Problem description

According to the arrangement of cables, two kinds of CDPRs can be considered. One is suspended CDPRs, where all the driven cables are above the end-effector and gravity acts as a virtual cable to keep equilibrium, such as the CoGiRo robot [32]. The other is non-

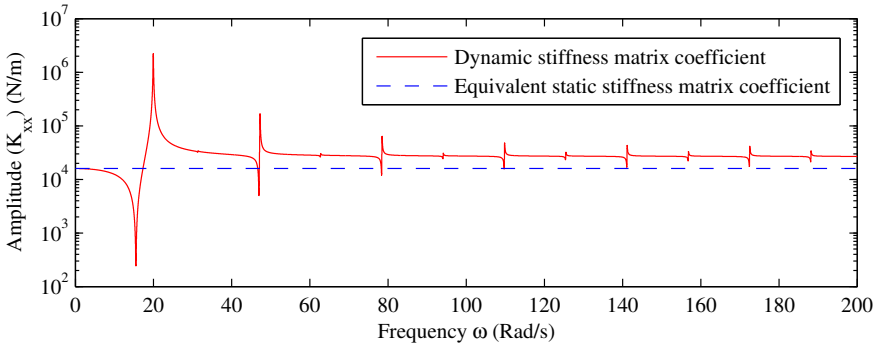

Fig. 2. The amplitude variation of a coefficient of the dynamic and static stiffness matrix for an example cable.

suspended CDPRs or fully constrained CDPRs, where at least one driven cable is below the end-effector, such as the FALCON robot [11,12].

For non-suspended CDPRs, sag-introduced flexibility can be reduced by increasing internal cable forces. As long as the internal cable forces are big enough, the effect of cable sag can be neglected, and the assumption of massless linear spring cable can be used in the static stiffness analysis. However, the method of increasing internal forces cannot be applied to suspended CDPRs. Because there does not exist a cable below the end-effector, and the cable forces mainly depend on the external load applied to the end-effector. Therefore, sag-introduced stiffness should be considered in the stiffness analysis of CDPRs, especially when the external load is small.

This paper mainly focuses on the suspended CDPRs. But the proposed method is also significant in the analysis of non-suspended CDPRs. In fact, increasing internal cable forces is a passive method, which leads directly the increase on motor power and energy consumption. In practical applications, it is impossible to eliminate sag-introduced flexibility entirely, especially for the CDPRs with heavy and long-span cables. Therefore, the proposed method is also useful for the stiffness analysis of non-suspended CDPRs.

Fig. 3 presents a general configuration of cable-suspended parallel robot, where:

- A_i is the attachment point in the end-effector and B_i is the attachment point in the fixed base;
- $\Re_G\ (O_G, x_G, y_G, z_G)$ is the fixed global frame;
- $\Re_e\ (O_e, x_e, y_e, z_e)$ is the local frame fixed on the end-effector;
- L_i is the i^{th} cable;
- $\Re_{B_i}(B_i, X, Y, Z)$ is parallel to $\Re_G\ (O_G, x_G, y_G, z_G)$;
- $\Re_{ci}\ (O_{ci}, x_{ci}, y_{ci}, z_{ci})$ is the local cable frame, where points O_{ci} and B_i are coincident, axis z_{ci} is parallel to z_G, axis x_{ci} is in the cable plane, and axis y_{ci} is perpendicular to the cable plane.

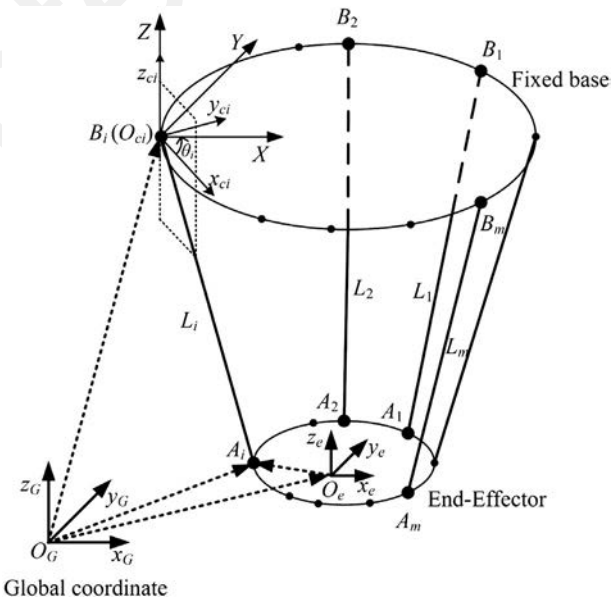

Fig. 3. General configuration of cable-suspended parallel robot.

3.2. Static stiffness analysis of CDPRs

For CDPRs using massless spring cable model, the platform pose error can be calculated by its static Cartesian stiffness matrix, assuming the compliant displacements of the platform are small [5]. However, with non-negligible cable mass, sag-introduced flexibility should be considered, and the small compliant displacement assumption is no longer valid. Therefore, the Cartesian stiffness matrix cannot be used to calculate the pose error. Here, the kinematic model of CDPRs is used to define the pose error of the end-effector. In this section, the kinematic model is firstly presented, then the variation of the end-effector pose error with the external load is defined as an index for the static stiffness evaluation.

3.2.1. Kinematic model

3.2.1.1. a) ***Inverse kinematics***. The objective of inverse kinematics is to get all the actuated cable lengths for a given pose of the end-effector. If the cable mass and elasticity cannot be neglected, the inverse kinematics of CDPRs is coupled with the static equilibrium, which means that the cable lengths and the cable forces must be solved at the same time. The procedures of solving inverse kinematics are as following:

(1) *Get the coordinate of A_i in the cable frame $\mathfrak{R}_{ci}$* (equations from geometric relationship)
The coordinate of A_i in the global frame $\mathfrak{R}_G$ is:

$$\overrightarrow{{}^{G}O_GA_i} = \overrightarrow{{}^{G}O_GO_e} + \overrightarrow{{}^{G}O_eA_i} = \overrightarrow{{}^{G}O_GO_e} + {}^{G}\mathbf{T}_e\,\overrightarrow{{}^{e}O_eA_i}, \tag{21}$$

where ${}^{G}\mathbf{T}_e$ is the rotation matrix that transfers the coordinates in $\mathfrak{R}_e$ to their corresponding coordinates in $\mathfrak{R}_G$.
The coordinate of A_i in the cable frame $\mathfrak{R}_{ci}$ is:

$$\overrightarrow{{}^{ci}O_{ci}A_i} = {}^{G}\mathbf{T}_{ci}^{-1}\,\overrightarrow{{}^{G}O_{ci}A_i} = {}^{G}\mathbf{T}_{ci}^{-1}\left(\overrightarrow{{}^{G}O_GA_i} - \overrightarrow{{}^{G}O_GO_{ci}}\right), \tag{22}$$

where ${}^{G}\mathbf{T}_{ci}$ is the rotation matrix that maps the coordinates in $\mathfrak{R}_{ci}$ to their corresponding coordinates in $\mathfrak{R}_G$.

(2) *Equations from the static cable model*
The coordinates of A_i in the cable frame $\mathfrak{R}_{ci}$ can also be obtained by substituting $s = l_{usi}$ into Eqs. (9) and (10):

$$x_{\overrightarrow{O_{ci}A_i}} = x(l_{usi}) = \frac{f_{Axi}l_{usi}}{EA} + \frac{|f_{Axi}|}{\rho g}\left[sinh^{-1}\left(\frac{f_{Azi}}{f_{Axi}}\right) - sinh^{-1}\left(\frac{f_{Azi}-\rho g l_{usi}}{f_{Axi}}\right)\right], \tag{23}$$

$$z_{\overrightarrow{O_{ci}A_i}} = z(l_{usi}) = \frac{f_{Azi}l_{usi}}{EA} - \frac{\rho g l_{usi}^2}{2EA} + \frac{1}{\rho g}\left[\sqrt{f_{Axi}^2 + f_{Azi}^2} - \sqrt{f_{Axi}^2 + (f_{Azi}-\rho g l_{usi})^2}\right], \tag{24}$$

where $i = 1, 2, \cdots m$. For a CDPR driven by m cables, the number of equations from the static cable model is $2m$.

(3) *Equations from static equilibrium of the end-effector*
The equations for static equilibrium of the end-effector are:

$$\overrightarrow{{}^{G}F_{Ai}} + \overrightarrow{{}^{G}F_{ex}} = \vec{0}, \tag{25}$$

$$\overrightarrow{{}^{G}O_eA_i} \times \overrightarrow{{}^{G}F_{Ai}} + \overrightarrow{{}^{G}M_{ex}} = \vec{0}, \tag{26}$$

where $\overrightarrow{{}^{G}F_{ex}}$ and $\overrightarrow{{}^{G}M_{ex}}$ are respectively the external forces and moments expressed in global frame. $\overrightarrow{{}^{G}F_{Ai}}$ are the forces exerted by the cables on the end-effector at points A_i, and $\overrightarrow{{}^{G}F_{Ai}} = {}^{G}\mathbf{T}_{ci}\,\overrightarrow{{}^{ci}F_{Ai}}$, $\overrightarrow{{}^{ci}F_{Ai}} = [-f_{Axi}\,0\,-f_{Azi}]^T$. For a CDPR of n DOFs, the number of static equilibrium equations is n, where $n \le 6$.

(4) *Solving the equations*
As the coupling of the cable forces and the cable lengths, there is no analytic solution for the above nonlinear equations. So optimization methods are employed. The 'fmincon' function in Matlab [1] is used to solve Eqs. (23) to (26). The unknowns in the equations are: $l_{usi}, f_{Axi}, f_{Azi}$ $(i = 1, 2 \cdots m)$. Finally, there are $3m$ unknowns and $2m + n$ equations.
There are three cases according to the relationship between m and n.

1. $m = n$, there are as many unknowns as the equations.
2. $m < n$, there are more equations than the unknowns, and the solutions may not exist. This means that the end-effector cannot be positioned arbitrarily in 6 DOFs.

[1] Matlab is software of MathWorks® company (http://www.mathworks.com).

3. $m > n$, the unknowns outnumber the equations, so the solution will not be unique. In this case, different sets of cable lengths and forces can be obtained for the same given pose of the end-effector. To make the solution unique, constrained optimization with a cost function can be used.

(5) *Initial guess for the iteration*

Good initial guess is important for the convergence and the efficiency of the optimization method. Assuming that cables are ideal straight lines without mass and elasticity, thus the cable forces and cable lengths are uncoupled. The ideal cable lengths can be calculated through the inverse kinematics ($l_{0i} = |\overrightarrow{A_iB_i}|$). The ideal cable forces can be calculated through the static equilibrium ($\mathbf{J}^T\mathbf{F} + \mathbf{W}_{ex} = 0$), where $\mathbf{J}^T$ is the transposition of Jacobian matrix, $\mathbf{F} = [f_{A1}f_{A2}\cdots f_{Am}]^T$ is the ideal cable forces, and $\mathbf{W}_{ex}$ is the external wrench (force and moment) applied on the end-effector. Then the calculated cable lengths and forces can be used as the initial guess.

During the calculation of cable forces, three cases should be considered according to the rank of $\mathbf{J}^T$:

1. $m = n$, $\mathbf{J}^T$ is full rank and reversible except for the singulary poses. The ideal cable forces can be calculated by $\mathbf{F} = -\mathbf{J}^{-T}\mathbf{W}_{ex}$.
2. $m < n$, $\mathbf{J}^T$ is not full rank. There are more equations than variables in $\mathbf{J}^T\mathbf{F} + \mathbf{W}_{ex} = 0$. The ideal cable forces $\mathbf{F}$ can be calculated by choosing any m equations from the n equations. Then the solution should be substituted back into the remaining $n - m$ equations to be tested.
3. $m > n$, $\mathbf{J}^T$ is not full rank. There are less equations than variables in $\mathbf{J}^T\mathbf{F} + \mathbf{W}_{ex} = 0$. Different force distribution methods [33–35] can be used to calculate the ideal cable forces.

3.2.1.2. b) ***Direct kinematics***. The objective of direct kinematics is to get the pose of the end-effector for a given set of actuated cable lengths. The constraints of direct kinematics are the same with that of inverse kinematics (Eqs. (23) to (26)). With non-negligible cable mass and elasticity, the direct kinematics is coupled with the static equilibrium. The end-effector pose and the cable forces should be calculated at the same time. For an n DOFs CDPR with m cables, there are $2m + n$ equations (Eqs. (23) to (26)) and $2m + n$ unknown variables. Various kinds of methods can be used for solving the direct kinematic problem [36–38]. In this paper, optimization method is used to solve the direct kinematic problem.

3.2.2. Static pose error definition

Fig. 4 presents the definition of the pose error of the end-effector. For a given set of unstrained cable lengths l_{usi}, the pose (position and orientation) of the end-effector can be obtained through direct kinematic model. In the modeling of direct kinematics, different cable models can be used, such as the ideal cable model where the cable is considered to be an inextensible straight line, the spring cable model where the cable is simplified as linear spring without mass, and the sagging cable model where elastic catenary is employed considering both cable mass and elasticity. The difference between the pose obtained through the spring cable model or the sagging cable model and the reference pose obtained through the ideal cable model defines the static pose error of the robot. It should be noted that the cable lengths l_{usi} are not given arbitrarily. In fact, it is a two step procedure. Firstly, a pose of the end-effector in its workspace is chosen as a reference. Then the reference cable lengths are obtained from the ideal inverse kinematics model, and the set of cable lengths l_{usi} is given according to the reference lengths. In this way, the reference pose of the end-effector can be used as a good initial guess for the direct kinematics.

In this paper, the variation of the end-effector pose error is regarded as the index for static stiffness evaluation. First of all, this method is simple. It has a direct natural interpretation as it is associated with the compliant displacement of the end-effector under the effect of external load. Furthermore, the static stiffness of CDPRs has two sources: sag-introduced flexibility and axial cable flexibility. The variation of the end-effector pose error calculated by the sagging cable model presents the global system stiffness. While the variation of the end-effector pose error calculated by the spring cable model only reflects the contribution of axial cable flexibility to the system stiffness. The difference between the results obtained by sagging cable model and the results by spring cable model expresses the contribution of sag-introduced flexibility. Thus, the effect of each source on the system stiffness can be clearly defined. In addition, pose error is easy to measure, which is convenient for experimental validation. It should be noticed that stiffness matrix and its mathematical properties are also powerful for stiffness analysis (as illustrated in [21]). In this paper, these two methods are not compared with each other.

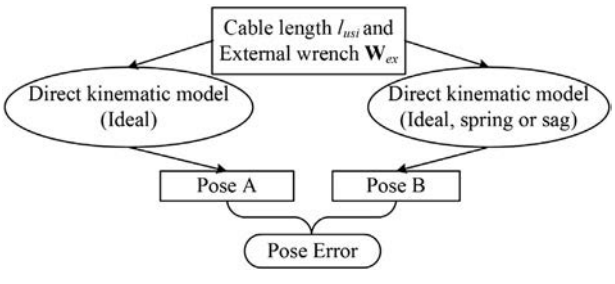

Fig. 4. Static pose error definition.

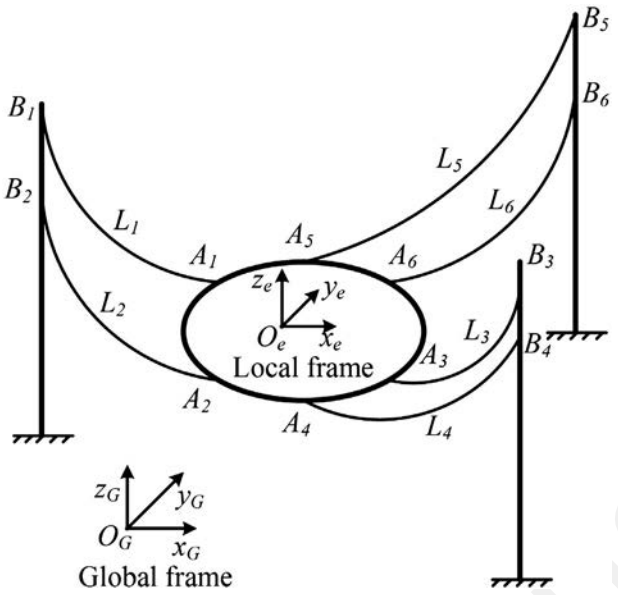

Fig. 5. A 6-DOF CDPR prototype.

3.3. Dynamic stiffness analysis of CDPRs

A new dynamic stiffness model of CDPRs is proposed in this section. This model is based on the DSM method. Firstly, the dynamic stiffness matrix of CDPRs is calculated by assembling the dynamic matrix of the driven cables. Then system dynamic equation is formulated and the Frequency Response Functions (FRFs) are calculated to identify the robot natural frequencies.

3.3.1. Computation of dynamic stiffness matrix

Eq. (20) gives the dynamic stiffness matrix of a single cable ${}^{ci}\mathbf{K}_i(\omega)$ in its local cable frame $\mathfrak{R}_{ci}$. As the robot stiffness is affected by all the driven cables, it is necessary to express the cable stiffness matrix in the global frame $\mathfrak{R}_G$ (Fig. 3).

$$ {}^{G}\mathbf{K}_i(\omega) = {}^{G}\mathbf{T}_{ci}\,{}^{ci}\mathbf{K}_i(\omega)\,{}^{G}\mathbf{T}_{ci}^{-1}. \tag{27} $$

Then the stiffness matrix of the robot ${}^{G}\mathbf{K}_M(\omega)$ can be assembled by considering all driven cables:

$$ {}^{G}\mathbf{K}_M(\omega) = \sum_{i=1}^{m} \mathbf{A}_i^{T}\,{}^{G}\mathbf{K}_i(\omega)\mathbf{A}_i, \tag{28} $$

where:

$$ \mathbf{A}_i = \begin{bmatrix} 1 & 0 & 0 & 0 & -z_{\overrightarrow{o_eA_i}} & y_{\overrightarrow{o_eA_i}} \\ 0 & 1 & 0 & z_{\overrightarrow{o_eA_i}} & 0 & -x_{\overrightarrow{o_eA_i}} \\ 0 & 0 & 1 & -y_{\overrightarrow{o_eA_i}} & x_{\overrightarrow{o_eA_i}} & 0 \end{bmatrix}. \tag{29} $$

Furthermore, the robot stiffness matrix can also be expressed as ${}^{e}\mathbf{K}_M(\omega)$ in the end-effector frame $\mathfrak{R}_e$ using the rotation matrix ${}^{G}\mathbf{T}_e$.

Table 1
Configuration parameters: coordinates of the points B_i in global frame and that of A_i in local frame.

(m)	x	y	z		x	y	z
A_1	−0.025	−0.143	0	B_1	5.327	−2.267	4.193
A_2	0.136	−0.050	0	B_2	5.327	−2.267	3.822
A_3	0.136	0.050	0	B_3	5.327	2.267	4.193
A_4	−0.025	0.143	0	B_4	5.327	2.267	3.822
A_5	−0.111	0.093	0	B_5	−5.775	0.010	4.193
A_6	−0.111	−0.093	0	B_6	−5.775	0.010	3.822

Table 2
Cable parameters.

Diameter		4 mm			8 mm		
Length	l_{us1} – l_{us3}	6863	6565	6756	4859	4552	4830
(mm)	l_{us4} – l_{us6}	6663	6801	6604	4586	9417	9284
Young's modulus		19.9 GPa			20.1 GPa		
Mass per meter		0.067 kg/m			0.251 kg/m		

3.3.2. Natural frequency identification

For CDPRs, the system stiffness is mainly affected by the stiffness of their cables, actuators, and end-effector. Compared with cables, the compliance of the actuators and the end-effector is much lower and therefore neglected. The free vibration equations of a CDPR can be written as:

$$\mathbf{M}\ddot{\overline{\mathbf{x}}}(t)+{}^{e}\mathbf{K}_{M}(\omega)\overline{\mathbf{x}}(t)=0, \tag{30}$$

where $\overline{\mathbf{x}}(t)$ represents the perturbation of the end-effector in position and orientation from the static equilibrium. $\mathbf{M}$ is the 6 by 6 mass matrix of the end-effector.

In the previous study [19,26,28], cable mass is neglected on the vibration analysis. The system stiffness matrix ${}^{e}\mathbf{K}_{M}$ is constant in frequency. According to the free vibration theory of multi-degree-of-freedom system, the natural frequencies of the CDPR can be calculated by transforming system dynamic equation into its modal space, and then solving the classic eigenvalue and eigenvector problems.

However, in this paper, both cable mass and elasticity are considered. As a result, the system stiffness matrix ${}^{e}\mathbf{K}_{M}(\omega)$ is function of the frequency ω. The above method for linear multi-degree-of-freedom system is not suitable. The analysis of the dynamic response functions of the robot to a harmonic excitation can be used.

For each pose of the end-effector path, the dynamic equation of a CDPR under a harmonic excitation can be written as:

$$\mathbf{M}\ddot{\overline{\mathbf{x}}}(t)+{}^{e}\mathbf{K}_{M}(\omega)\overline{\mathbf{x}}(t)=\mathbf{F}e^{j\omega t}. \tag{31}$$

Assuming that the vibration response of the end-effector is $\overline{\mathbf{x}}(t)=\mathbf{X}e^{j\omega t}$, the solution of Eq. (31) can be written as:

$$\mathbf{X}=\left[-\omega^{2}\mathbf{M}+{}^{e}\mathbf{K}_{M}(\omega)\right]^{-1}\mathbf{F}. \tag{32}$$

The dynamic amplification due to resonance will enable to identify the robot natural frequencies.

4. Experimental validation

In this section, a 6-DOF suspended CDPR is presented as an example to verify the proposed method. The effects of cable mass and elasticity on the static and dynamic stiffness performances are investigated by simulations and experiments.

The configuration of the prototype is similar to the CDPR presented in [2]. There are 6 attachment points on the three vertical poles and 6 attachment points on the end-effector (Fig. 5). These points are connected by 6 cables. The dimensions of this prototype are about 10 m long, 6 m wide and 5 m high. Table 1 gives the detailed parameters of the 6-DOF CDPR prototype. Because the purpose of this prototype is to verify the effect of cable sag on the stiffness characteristics of CDPRs at some poses in the workspace, the prototype is built without motors and winches. The attachment points are fixed on the top of the poles. Two sets of anti-rust steel cables are used. One set is ϕ4 mm in diameter and 6863, 6565, 6756, 6663, 6801, and 6604 mm in length. The other set is ϕ8 mm in diameter and 4859, 4552, 4830, 4586, 9417, and 9284 mm in length. Thus two poses of the end-effector can be achieved. The coordinates of the end-effector center in the global frame $\mathfrak{R}_{G}$ are (0, 0, 0.5 m) and (3, 0, 0.5 m) respectively, and the rotational angles are zeros. The cable Young's modulus is identified using a material testing machine. All the cables work within their linear elastic region. The relevant cable parameters are given in Table 2.

4.1. Static experiments

In order to study the static stiffness performance of CDPRs, experiments are carried out in this section. The effect of cable sag on the static stiffness behavior is validated, and the variation of system stiffness with external load is presented.

The experimental setup (Fig. 6) consists of the 6-DOF cable robot, a precise multi-camera system for tracking the pose of the end-effector and a loading device connected to the center of the end-effector. The measurement device is the Nikon Metrology K600-10 system [2] based on three CCD linear cameras and infra-red light active LEDs. Three LEDs are attached to the end-effector and its

[2] This is a product of Nikon® company: http://www.nikonmetrology.com.

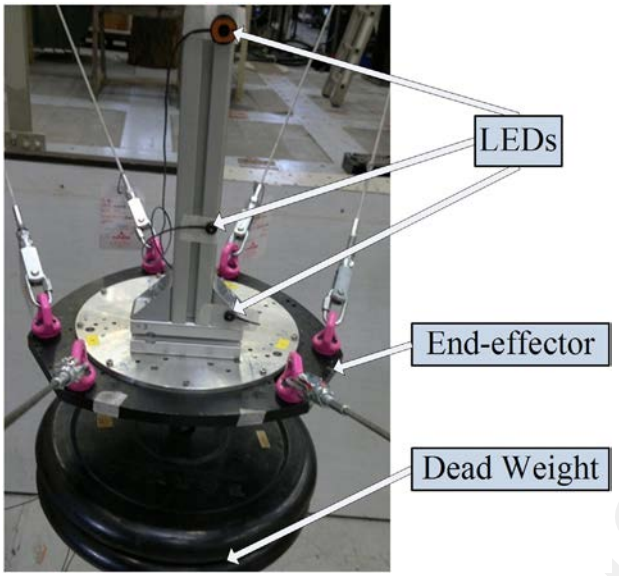

Fig. 6. Static experimental setup.

poses (both position and orientation) are measured by the camera. The system has a position measuring accuracy up to ± 37 μm for a single point. The mass of the end-effector can be adjusted from 10 to 86 kg by adding dead weights as shown in Fig. 6.

Fig. 7 shows the variation of the pose error of the end-effector along z-axis with the external load. Firstly, it is shown that the experimental data are quite close to the computational data obtained by the sagging cable model. Through these data, the effect of cable sag on the static stiffness of CDPRs is validated by experiment for the first time. In addition, the effect of external load on the static stiffness is illustrated. When the external load is small, the variation of the end-effector pose error with the external load is quite big, which means that the system stiffness is low. Also, there is a big difference between the pose error calculated by the sagging cable model and that by the spring cable model, which indicates that the sag-introduced cable flexibility is the main source of system stiffness. In this case, the sagging cable model is necessary to have a good evaluation for the system stiffness. After the external load increases beyond a certain value, the variation of the end-effector pose error with the external load becomes much smaller, and the results obtained by the sagging cable model are quite close to that by the spring model. This means that the system stiffness becomes higher and the sag-introduced flexibility is negligible. In this case, both the sagging model and the spring model have a good evaluation for system stiffness.

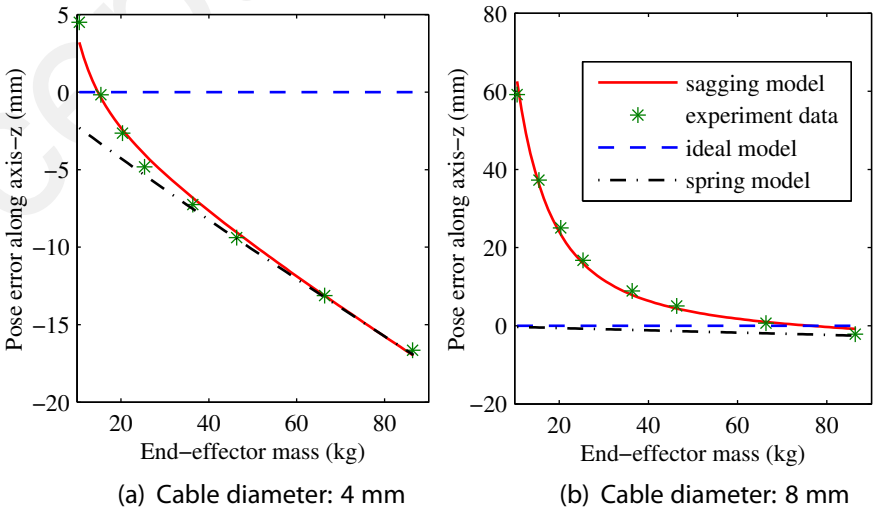

Fig. 7. Effect of external load on the static pose error of the CDPR prototype.

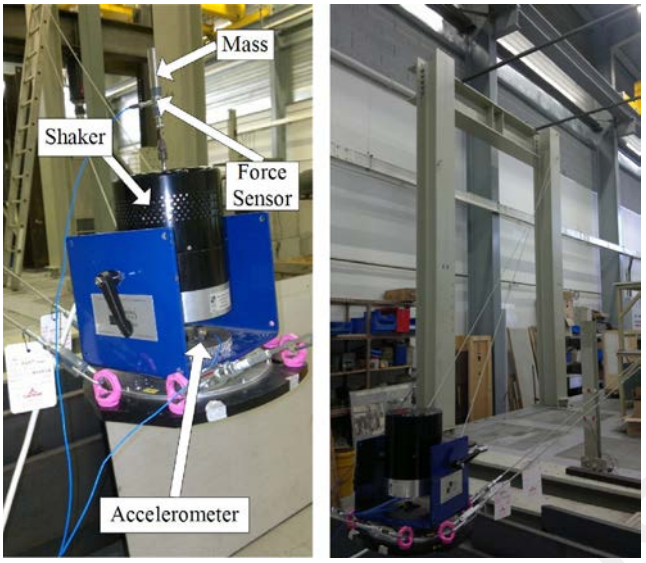

(a) End-effector (b) The 6-DOF CDPR prototype

Fig. 8. Dynamic experimental setup.

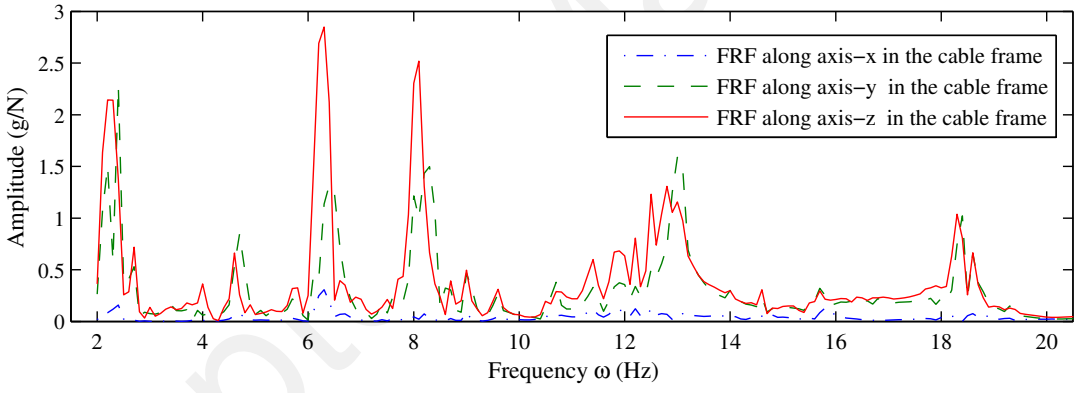

(a) Cable L_5: 8 mm in diameter

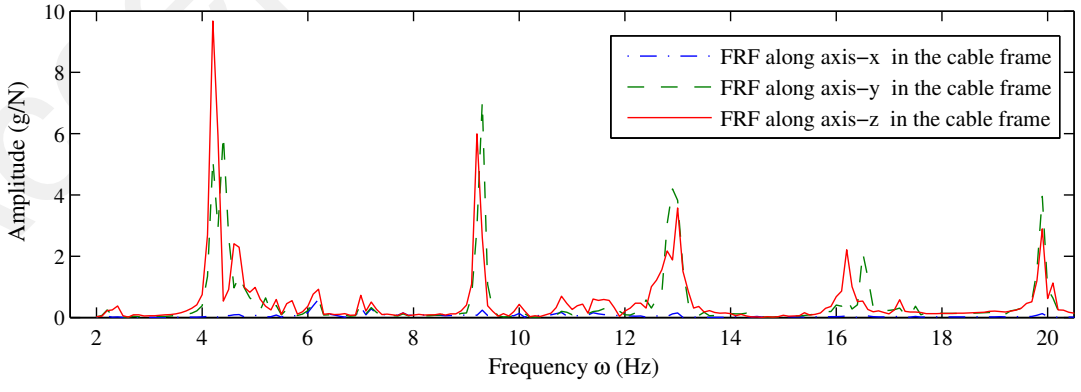

(b) Cable L_5: 4 mm in diameter

Fig. 9. Frequency Response Functions between the cable acceleration response and the excitation force.

Table 3
Cable natural frequency identification.

Diameter	Data sources	Cable natural frequencies (range: 2–20 Hz)											
4 mm cable	Experiment (±0.1 Hz)	4.4			9.3			13.1			16.5		19.9
	Dynamic stiffness matrix	4.9			9.9			14.9			19.9		24.8
Diameter	Data sources	Cable natural frequencies (range: 2–20 Hz)											
8 mm cable	Experiment (±0.1 Hz)	2.4	4.7	6.3	8.1	9.0	9.6	11.4	12.2	12.5	14.6	15.7	18.6
	Dynamic stiffness matrix	2.5	4.9	7.4	7.4	9.9	9.9	12.4	12.4	12.4	14.8	17.3	19.8

4.2. Dynamic experiments

In order to verify the dynamic stiffness model proposed in Section 3, tests have been performed to identify the dynamic characteristics of the 6-DOF CDPR prototype. Fig. 8 represents the experimental setup. It contains the 6-DOF cable robot, the two sets of steel cables, an electro-dynamic shaker, several sensors, the data acquisition and analysis system. As shown in Fig. 8(a), the shaker is mounted on the end-effector. A small mass block is fixed to the mobile stick of the shaker. A force sensor lies between the mass block and the mobile stick. Thus, the shaker can deliver a vertical force to the end-effector. The force is proportional to the acceleration amplitude of the mass block, and can be measured by the force sensor. A triaxial accelerometer is fixed on the platform. It is used to obtain the response of the end-effector along three mutually perpendicular directions. Several other accelerometers are fixed along the cables. The weight of the accelerometer is 5.8 g. Compared to the linear weight of the cables (67 g/m for 4 mm cable, and 251 g/m for 8 mm cable), its weight can be negligible. The total mass of the end-effector and other equipments fixed on it is 30 kg, with a rotational inertia $I_{xx} = 0.9, I_{yy} = 0.9$ and $I_{zz} = 0.77$ kg m^2 measured in the end-effector frame $\mathfrak{R}_e$. The cable parameters are listed in Table 2.

Experiments have been performed with a stepped sine excitation, i.e. a harmonic excitation at a fixed frequency changed step by step. The step size is 0.05 Hz. At each step, there is a stabilization time of 8 s. As the low-order natural frequencies are important to

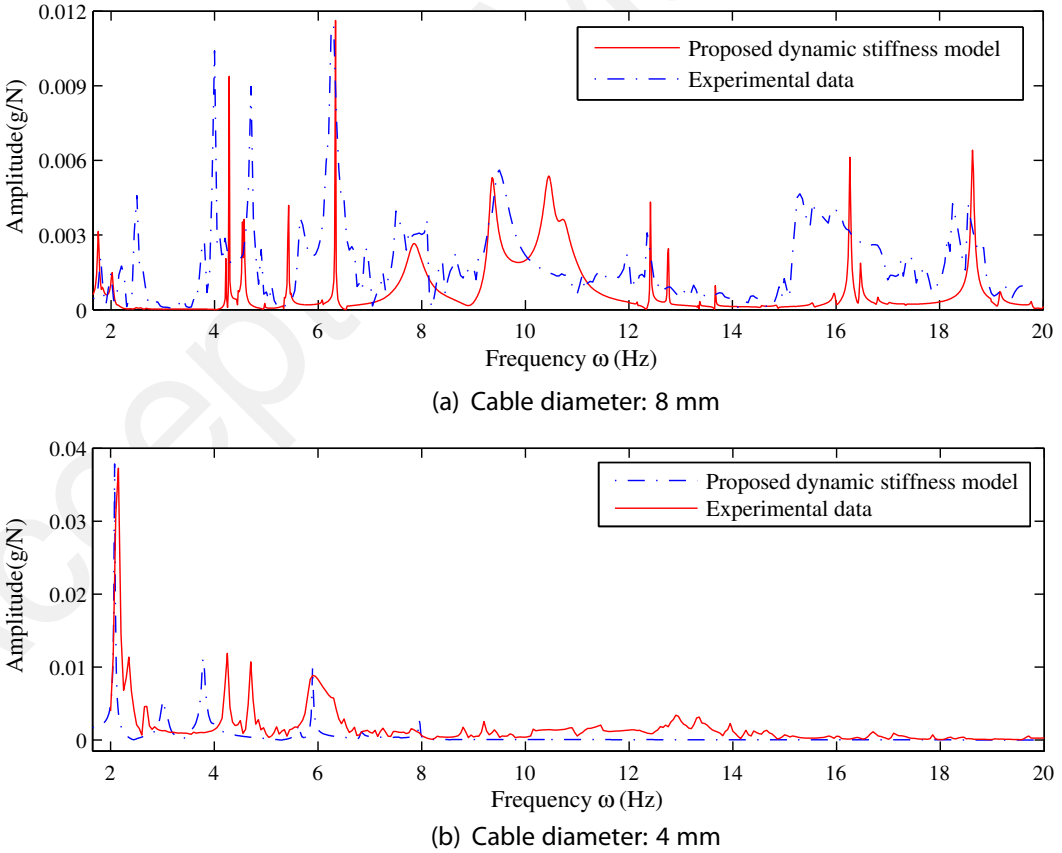

Fig. 10. Frequency Response Function between the acceleration response of the platform along y-axis and the excitation force along z-axis in the end-effector frame $\mathfrak{R}_e$.

Table 4
Robot's natural frequency comparison among different methods.

Diameter	Data sources	Robot's natural frequencies (range: 2–20 Hz)															
4 mm cable	Experiment (±0.1 Hz)	2.2			2.7			4.2			4.7			5.9			7.8
	Proposed dynamic model	2.1			3.0			3.8			3.8			5.9			7.9
	Static sagging model [19]	2.3			3.9			4.5			6.6			8.6			–
	Massless spring model [28]	2.5			4.0			4.8			7.8			9.1			–

Diameter	Data sources	Robot's natural frequencies (range: 2–20 Hz)															
8 mm cable	Experiment (±0.1 Hz)	2.0	2.5	4.0	4.7	5.6	6.3	7.7	8.6	9.5	11.1	12.0	12.3	13.8	15.3	18.5	
	Proposed dynamic model	2.0	2.0	4.3	4.6	5.4	6.3	7.8	9.4	9.4	10.5	12.4	12.8	13.7	16.3	18.6	
	Static sagging model [19]	2.1	4.6	6.0	7.7	11.1	–	–	–	–	–	–	–	–	–	–	
	Massless spring model [28]	2.8	5.6	8.2	9.5	15.8	18.2	–	–	–	–	–	–	–	–	–	

evaluate the dynamic stiffness of CDPRs, the dynamic experiment mainly focuses on the low frequency. However, the electro-dynamic shaker is not suitable for the dynamic test below 2 Hz. Therefore, the examined frequency range in this section is 2–20 Hz.

As explained before, we consider the Frequency Response Function (FRF) plot as a useful tool when dealing with resonance identification for non-linear system. The FRF plots presented in Fig. 9 have been calculated referring to the output of the accelerometers fixed along the cable and the output of the force sensor in the cable frame $\mathfrak{R}_{ci}$. It should be noticed that Fig. 9 presents the results of the cable L_5. Similar measurements are made for another two cables, L_4 and L_6. Conclusions are the same. For the sake of brevity, only the results for cable L_5 are given in this paper. From these FRF plots, it is possible to identify the natural frequencies of the cables through the resonances. Table 3 compares the cable natural frequencies identified by the FRF plots with those calculated using the cable dynamic stiffness matrix (Section 2.2). The correlation between the theoretical model and the experimental data is good for the low frequencies, but there exists some difference for the high frequencies. The CDPR prototype consists of the 6 cables and the end-effector. In the experiment, each cable is not isolated, but relevant with the end-effector and the other cables. Therefore, the cable response in the FRF plot can be affected by the response of other cables and/or the end-effector. In addition, as we can see from Fig. 9 and Table 3, the correlation for ϕ4 mm cable is better than that of ϕ8 mm cable. This can be explained by the smaller ε of the ϕ4 mm cable. As presented in Section 2.2, ε is the ratio between the horizontal cable weight and the cable tension. It is positively relevant to the cable sag. The cable dynamic stiffness matrix is based on the assumption of linear theory and small cable sag. Big cable sag can increase the non-linearity of the cable, and result in error of the theoretical model. The tension of the two cables is almost the same, 278 N for the ϕ4 mm cable and 264 N for the ϕ8 mm cable. But there exists a big difference on the horizontal cable weight, 4.2 N for the ϕ4 mm cable and 16.1 N for the ϕ8 mm cable. Thus it leads to an obvious difference in the value of ε: $\varepsilon = 0.013$ for the ϕ4 mm cable and $\varepsilon = 0.053$ for the ϕ8 mm cable. Therefore, the sag of the ϕ4 mm cable is smaller due to the smaller value of ε, and the correlation is better. In spite of this, the relative error is less than 20% for the first five modes.

As presented in Fig. 10, the FRF plots have been calculated referring to the acceleration response of the platform along y-axis and the excitation force of the shaker along z-axis in the end-effector frame $\mathfrak{R}_e$. The 6-DOF CDPR prototype exhibits several damped modes in the frequency range studied. The natural frequencies of the prototype with 4 mm cables and 8 mm cables are identified respectively. Results are listed in the first line of Table 4. As we can see, the difference between experimental results and simulation results is less than 1 Hz in the studied frequency range. For the configuration with 4 mm cables, the difference is up to 0.9 Hz for the intermediate frequencies. In simulation, the mode at 3.8 Hz is a double mode. However, due to experimental errors (such as cable length, fixing device and etc.), these two modes are separated in the experiment (4.2 and 4.7 Hz). These results allow concluding that the proposed dynamic stiffness model of CDPRs is effective for the natural frequency identification, although some critical aspects remain. In the experimental setup, metal rings are used as joints to connect the cable and the end-effector. However it is assumed that the cable end is fixed on the end-effector in the simulation. The metal rings can affect the natural frequencies of the CDPR prototype. Also,

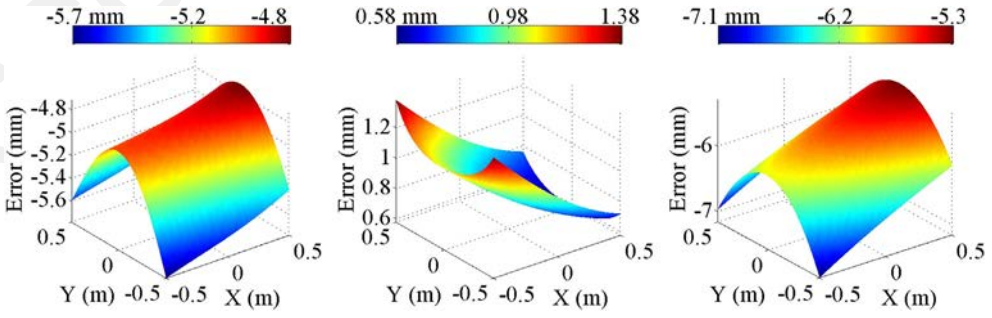

(a) Global pose error (b) Pose error caused by cable sag (c) Pose error caused by axial cable elasticity

Fig. 11. Static pose error of the end-effector along vertical direction over the sub-workspace for ϕ4 mm cable and 30 kg external load.

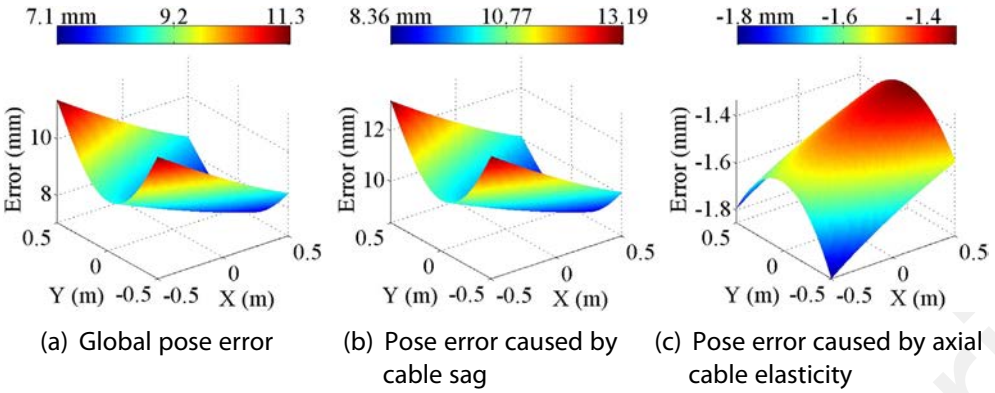

(a) Global pose error (b) Pose error caused by cable sag (c) Pose error caused by axial cable elasticity

Fig. 12. Static pose error of the end-effector along vertical direction over the sub-workspace for ϕ8 mm cable and 30 kg external load.

the cable damping ratio ξ is estimated as $0.01/(\frac{\rho}{\pi})$ [31]. Although the value of ξ has little effect on the robot natural frequencies, it can affect the amplitude of the FRF plots.

The results obtained by the dynamic stiffness model of the CDPR are compared with that obtained by the static sagging cable model [19] and the massless spring cable model [28]. The latter two models neglect the coupling between the end-effector dynamics and the cable resonances. From the comparison in Table 4, it is indicated that the dynamics of the cables change the value of natural frequencies and add new resonances. Furthermore, as we can see, the change of natural frequency between different models is more significant for ϕ8 mm cable than that for ϕ4 mm cable. This means that the effect of cable dynamics on system dynamic stiffness characteristics is more significant for heavier cable, as expected. Therefore, the evaluation of the dynamic stiffness of CDPRs should take cable dynamics into consideration, especially for heavy and/or long-span cables.

5. Application and discussion

Static and dynamic stiffness analyses are valuable and necessary to improve the performances of CDPRs, such as increasing the static positioning accuracy and attenuating the vibration in trajectory tracking. The proposed method for stiffness analysis in this paper is useful for design, optimization, identification, simulation and control purposes.

In previous sections, the effect of cable sag, cable mass and external load on the stiffness behavior of CDPRs is studied through simulations and experiments only for certain poses of the end-effector. As is known, the robot stiffness is also posture dependent. It is necessary to be considered over the workspace.

Figs. 11 and 12 present the pose error of the CDPR prototype along vertical direction over a sub-workspace with a fixed external load of 30 kg, for ϕ4 mm cable and ϕ8 mm cable respectively. The sub-workspace is defined by $-0.5\text{m} \leq X \leq 0.5\text{m}$, $-0.5\text{m} \leq Y \leq 0.5\text{m}$, $Z = 0.5$ m, and the rotational angles around axis-x, y, and z are all zeros. As we can see from Figs. 11(a) and 12(a), the static pose error of the end-effector varies significantly with the robot posture. The absolute value of the pose error tends to increase as the distance from the end-effector to the x-axis becomes larger. It tends to decrease as the end-effector moves along the positive direction of the x-axis. In addition, as explained in Section 4.1, the static pose error of CDPRs is caused by both cable sag and axial cable elasticity. Figs. 11(b) and 12(b) present the sag-introduced pose error of the end-effector along z-axis, while Figs. 11(c) and 12(c) present the pose error of the end-effector along z-axis caused by axial cable elasticity. As illustrated, the static pose error of the CDPR prototype is mainly dependent on the axial cable elasticity for CDPRs with ϕ4 mm cable (Fig. 11), while it is mainly dependent on the sag-introduced flexibility for CDPRs with ϕ8 mm cable (Fig. 12).

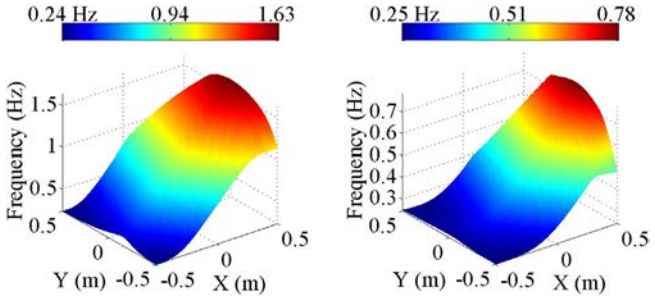

(a) φ4 mm cable and 30 kg external load (b) φ8 mm cable and 30 kg external load

Fig. 13. Dynamic stiffness evaluation through the first natural frequency of the prototype over the sub-workspace.

Figs. 13 and 14 present the dynamic stiffness evaluation of the CDPR prototype over the sub-workspace through the first natural frequency of the end-effector and the 6 driven cables respectively. As shown, the robot natural frequency varies with the end-effector pose. The first natural frequency of the end-effector with ϕ4 mm cable and 30 kg external load changes from 0.24 Hz to 1.63 Hz. While

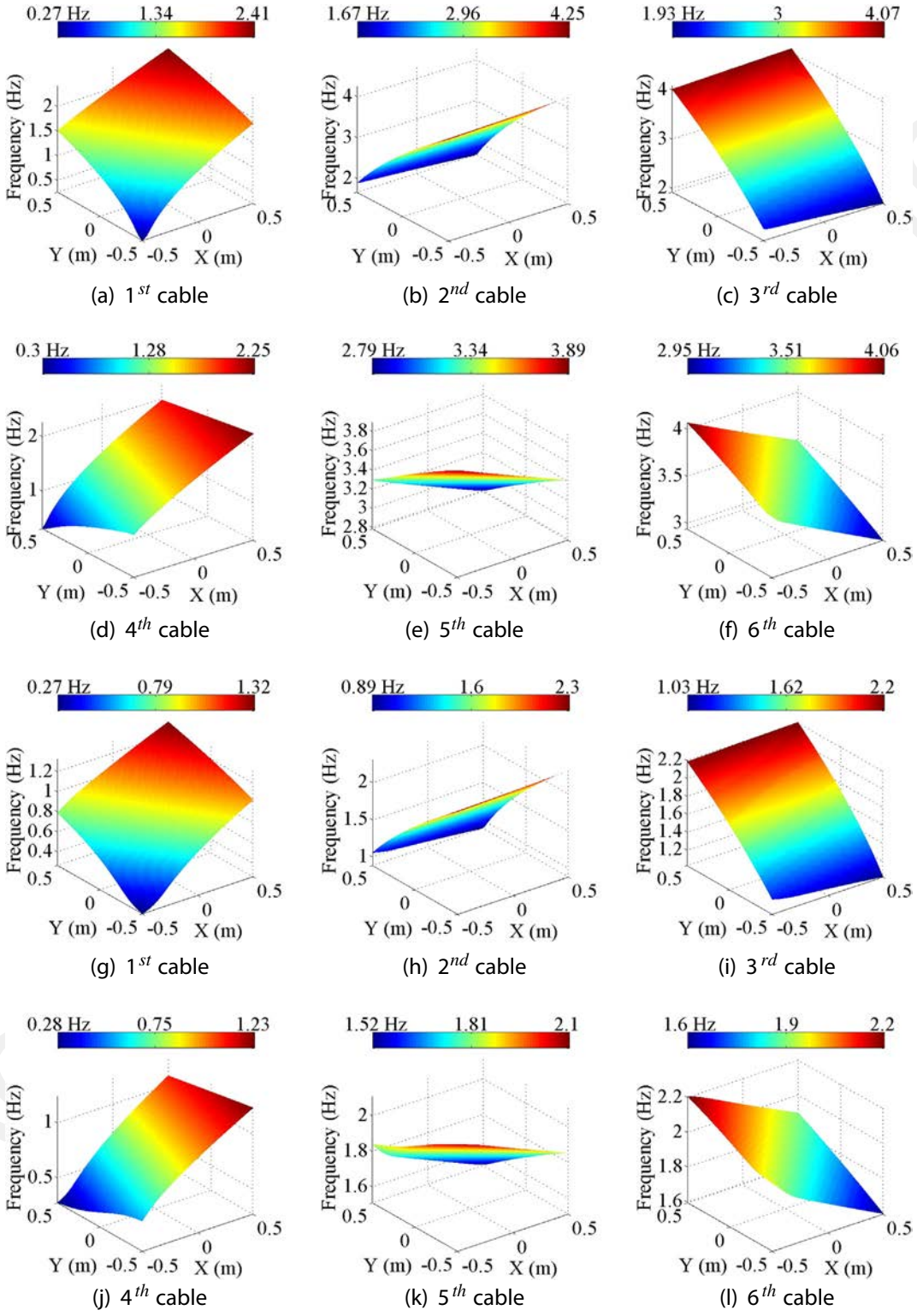

(a) 1 st cable (b) 2nd cable (c) 3 rd cable

(d) 4th cable (e) 5th cable (f) 6 th cable

(g) 1 st cable (h) 2nd cable (i) 3 rd cable

(j) 4 th cable (k) 5 th cable (l) 6 th cable

Fig. 14. First natural frequency of the cables over the sub-workspace: (a)–(f) is for ϕ4 mm cable, 30 kg external load; (g)–(l) is for ϕ8 mm cable, 30 kg external load.

for ϕ8 mm cable and 30 kg external load, the frequency varies from 0.25 Hz to 0.78 Hz. The end-effector natural frequency tends to increase as the robot moves along the positive direction of the x-axis.

The proposed method in this paper is helpful in the design procedures of CDPRs. It can help choosing the cable parameters, the end-effector mass, motor parameters, the control scheme and etc. Take a pick-and-place application of the suspended CDPRs for example. Using cables with lower density and/or higher Young's modulus is helpful to improve the stiffness of CDPRs. Keeping the trajectory in the center of the workspace can also increase their stiffness. Furthermore, stiffness can be enhanced with heavier end-effector. However, heavy end-effector will increase the power consumption and decrease the load capacity. Therefore it is necessary to choose suitable end-effector mass and cable parameters according to design requirements. In addition, an optimization of the control scheme can be made to ameliorate the stiffness performances of CDPRs. When the end-effector is empty, sag-introduced stiffness should be considered in the control model to get a good prediction of the end-effector pose. After picking up the cargo, the total mass of the end-effector becomes bigger and cable sag can be attenuated. Axial cable elasticity becomes the mainly source of the robot stiffness. A controller only considering axial cable elasticity can be used. It can accelerate calculation without losing accuracy.

For non-suspended CDPRs, the proposed method in this paper is also applicable. Increasing internal cable force can decrease cable sag and improve the stiffness of CDPRs. But larger cable force requires higher power motor and more energy supply. So a tradeoff between robot stiffness and cable force should be considered according to different application requirements. In addition, using light cable can weaken the effect of cable dynamics on robot dynamic stiffness. If the cable mass is negligible compared with the mass of the end-effector, spring cable model with axial elasticity can be used in the controller to simplify calculation and improve dynamic response. While cable mass is non-negligible, the coupling between cable dynamics and end-effector dynamics must be considered in the controller to ensure calculation accuracy.

For most applications of CDPRs, cable vibration is caused by internal factors, such as the acceleration of the end-effector and/or the winch, and the change of cable force and length during motion. However, for some applications, there exists external excitation on the cables of CDPRs, such as the wind-induced vibration problem of the large radio telescope (an application of the suspended CDPR [19]) and the wind-tunnel (an application of the non-suspended CDPR [23]). For these applications, external wind-induced excitation is the main reason for cable vibration. The cable resonance can directly lead to the vibration of the end-effector, and cable dynamics are strongly coupled with end-effector dynamics. In this case, cable dynamics (Fig. 14) should be considered to have a good evaluation of the CDPR performances.

6. Conclusion

This paper analyzes the static and dynamic stiffness of CDPRs with non-negligible cable mass and elasticity. Cable model is introduced. The static pose error of the end-effector is defined, and the variation of the end-effector pose error with the external load is used to evaluate the static stiffness of CDPRs. A new dynamic model of CDPRs is proposed, which is based on the dynamic stiffness matrix of a single cable. It considers the coupling of cable dynamics and end-effector vibration. Based on this dynamic model, robot natural frequencies are identified through the Frequency Response Functions of CDPRs, with the purpose of dynamic stiffness evaluation. Experiments are carried out on a 6-DOF CDPR prototype. The effect of cable sag and external load on the static stiffness of CDPRs is validated. Results show that sag-introduced flexibility is the main source of static robot stiffness with small external load, and axial cable flexibility becomes the main source with big external load. Vibration experiments are performed on the CDPR prototype. Dynamic response functions of the driven cables and the end-effector are calculated to identify the natural frequencies. Compared with other methods available in literature, it is indicated that cable dynamics have an obvious effect to the robot dynamic stiffness by changing the value of robot natural frequencies and/or add new resonances. In addition, static pose error and the first natural frequency of CDPRs over the workspace are calculated. Applications of suspended CDPRs and non-suspended CDPRs are discussed. Results show that the proposed method in this paper is useful for the design, simulation and control procedures of CDPRs. Our current and future work contains high-accurate trajectory tracking and active vibration control of CPRRs considering the effect of cable sag and elasticity.

References

[1] J.-P. Merlet, Parallel Robots, Springer, 2006.
[2] M. Gouttefarde, J. Collard, N. Riehl, C. Baradat, Simplified static analysis of large-dimension parallel cable-driven robots, IEEE International Conference on Robotics and Automation (ICRA), 2012, pp. 2299–2305.
[3] N. Riehl, M. Gouttefarde, S. Krut, C. Baradat, F. Pierrot, Effects of non-negligible cable mass on the static behavior of large workspace cable-driven parallel mechanisms, IEEE International Conference on Robotics and Automation (ICRA), 2009, pp. 2193–2198.
[4] C. Gosselin, Stiffness mapping for parallel manipulators, IEEE Trans. Robot. Autom. 6 (3) (1990) 377–382.
[5] G. Carbone, Stiffness analysis and experimental validation of robotic systems, Front. Mech. Eng. 6 (2) (2011) 182–196.
[6] E. Courteille, D. Deblaise, P. Maurine, Design optimization of a delta-like parallel robot through global stiffness performance evaluation, IEEE/RSJ International Conference on Intelligent Robots and Systems (IROS), 2009, pp. 5159–5166.
[7] D. Deblaise, X. Hernot, P. Maurine, A systematic analytical method for PKM stiffness matrix calculation, IEEE International Conference on Robotics and Automation (ICRA), 2006, pp. 4213–4219.
[8] B.S. El-Khasawneh, P.M. Ferreira, Computation of stiffness and stiffness bounds for parallel link manipulators, Int. J. Mach. Tools Manuf. 39 (2) (1999) 321–342.
[9] R. Verhoeven, M. Hiller, S. Tadokoro, Workspace, stiffness, singularities and classification of tendon-driven Stewart platforms, Advances in Robot Kinematics: Analysis and Control, Springer, Netherlands, 1998, pp. 105–114.
[10] N.G. Dagalakis, J.S. Albus, B.-L. Wang, J. Unger, J.D. Lee, Stiffness study of a parallel link robot crane for shipbuilding applications, J. Offshore Mech. Arct. Eng. 111 (3) (1989) 183.
[11] S. Kawamura, W. Choe, S. Tanaka, S. Pandian, Development of an ultrahigh speed robot FALCON using wire drive system, IEEE International Conference on Robotics and Automation (ICRA), vol. 1, 1995, pp. 215–220.

[12] S. Kawamura, H. Kino, C. Won, High-speed manipulation by using parallel wire-driven robots, Robotica 18 (1) (2000) 13–21.
[13] S. Behzadipour, A. Khajepour, Stiffness of cable-based parallel manipulators with application to stability analysis, J. Mech. Des. 128 (1) (2006) 303.
[14] M. Korayem, M. Bamdad, M. Saadat, Workspace analysis of cable-suspended robots with elastic cable, IEEE International Conference on Robotics and Biomimetics (ROBIO), 2007, pp. 1942–1947.
[15] Y. Bedoustani, H. Taghirad, M. Aref, Dynamics analysis of a redundant parallel manipulator driven by elastic cables, 10th International Conference on Control, Automation, Robotics and Vision (ICARCV), 2008, pp. 536–542.
[16] A. Vafaei, M. Khosravi, H. Taghirad, Modeling and control of cable driven parallel manipulators with elastic cables: Singular perturbation theory, in: S. Jeschke, H. Liu, D. Schilberg (Eds.), Intelligent Robotics and Applications, Lecture Notes in Computer Science, vol. 7101, Springer Berlin/Heidelberg, 2011, pp. 455–464.
[17] M.A. Khosravi, H.D. Taghirad, Robust PID control of cable-driven robots with elastic cables, First RSI/ISM International Conference on Robotics and Mechatronics (ICRoM), 2013, pp. 331–336.
[18] H.M. Irvine, Cable Structures, Dover Publications, 1992.
[19] K. Kozak, Q. Zhou, J. Wang, Static analysis of cable-driven manipulators with non-negligible cable mass, IEEE Trans. Robot. 22 (3) (2006) 425–433.
[20] J. Sandretto, G. Trombettoni, D. Daney, Confirmation of hypothesis on cable properties for cable-driven robots, in: F. Viadero, M. Ceccarelli (Eds.), New Trends in Mechanism and Machine Science, Mechanisms and Machine Science, vol. 7, Springer Netherlands, 2013, pp. 85–93.
[21] M. Arsenault, Workspace and stiffness analysis of a three-degree-of-freedom spatial cable-suspended parallel mechanism while considering cable mass, Mech. Mach. Theory 66 (2013) 1–13.
[22] B. Zi, B. Duan, J. Du, H. Bao, Dynamic modeling and active control of a cable-suspended parallel robot, Mechatronics 18 (1) (2008) 1–12.
[23] C. Sturm, L. Wildan, T. Bruckm, Wire Robot Suspension Systems for Wind Tunnels, InTech. (2010) 29–50.
[24] J. Du, H. Bao, C. Cui, D. Yang, Dynamic analysis of cable-driven parallel manipulators with time-varying cable lengths, Finite Elem. Anal. Des. 48 (1) (2012) 1392–1399.
[25] A.F. Tang, Y. Li, L.F. Kong, X.J. Cheng, Vibration analysis of tendon-based parallel robot for processing, Adv. Mater. Res. 655–657 (2013) 1086–1091.
[26] O. Ma, X. Diao, Dynamics analysis of a cable-driven parallel manipulator for hardware-in-the-loop dynamic simulation, IEEE/ASME International Conference on Advanced Intelligent Mechatronics (AIM), 2005, pp. 837–842.
[27] J. Du, W. Ding, H. Bao, Cable vibration analysis for large workspace cable-driven parallel manipulators, in: T. Bruckmann, A. Pott (Eds.), Cable-Driven Parallel Robots, no. 12 in Mechanisms and Machine Science, Springer, Berlin Heidelberg, 2013, pp. 437–449.
[28] X. Diao, O. Ma, Vibration analysis of cable-driven parallel manipulators, Multibody Sys.Dyn. 21 (4) (2009) 347–360.
[29] A. Ansell, The dynamic element method for analysis of frame and cable type structures, Eng. Struct. 27 (13) (2005) 1906–1915.
[30] J. Kim, S.P. Chang, Dynamic stiffness matrix of an inclined cable, Eng. Struct. 23 (12) (2001) 1614–1621.
[31] U. Starossek, Dynamic stiffness matrix of sagging cable, J. Eng. Mech. 117 (12) (1991) 2815–2828.
[32] T. Dallej, M. Gouttefarde, N. Andreff, R. Dahmouche, P. Martinet, Vision-based modeling and control of large-dimension cable-driven parallel robots, IEEE/RSJ International Conference on Intelligent Robots and Systems (IROS), 2012, pp. 1581–1586.
[33] A. Pott, T. Bruckmann, L. Mikelsons, Closed-form force distribution for parallel wire robots, in: A. Kecskemthy, A. Miller (Eds.), Computational Kinematics, Springer Berlin Heidelberg, 2009, pp. 25–34.
[34] L. Mikelsons, T. Bruckmann, M. Hiller, D. Schramm, A real-time capable force calculation algorithm for redundant tendon-based parallel manipulators, Robotics and Automation, 2008, ICRA 2008. IEEE International Conference on, 2008, pp. 3869–3874.
[35] C. Gosselin, M. Grenier, On the determination of the force distribution in overconstrained cable-driven parallel mechanisms, Meccanica 46 (1) (2011) 3–15.
[36] A. Pott, An algorithm for real-time forward kinematics of cable-driven parallel robots, in: J. Lenarcic, M.M. Stanisic (Eds.), Advances in Robot Kinematics: Motion in Man and Machine, Springer Netherlands, 2010, pp. 529–538.
[37] J. von Zitzewitz, G. Rauter, H. Vallery, A. Morger, R. Riener, Forward kinematics of redundantly actuated, tendon-based robots, Intelligent Robots and Systems (IROS), 2010 IEEE/RSJ International Conference on, 2010, pp. 2289–2294.
[38] A. Berti, J.-P. Merlet, M. Carricato, Solving the direct geometrico-static problem of 3-3 cable-driven parallel robots by interval analysis: preliminary results, in: T. Bruckmann, A. Pott (Eds.), Cable-driven parallel robots, Mechanisms and Machine Science, vol. 12, Springer Berlin Heidelberg, 2013, pp. 251–268.